Cell Reports
Report

Impaired Dendritic Expression and Plasticity of h-Channels in the *fmr1*$^{-/y}$ Mouse Model of Fragile X Syndrome

Darrin H. Brager,[1,*] Arvin R. Akhavan,[1] and Daniel Johnston[1]
[1]Center for Learning and Memory, The University of Texas at Austin, Austin, TX 78712, USA
*Correspondence: dbrager@mail.clm.utexas.edu
DOI 10.1016/j.celrep.2012.02.002

SUMMARY

Despite extensive research into both synaptic and morphological changes, surprisingly little is known about dendritic function in fragile X syndrome (FXS). We found that the dendritic input resistance of CA1 neurons was significantly lower in *fmr1*$^{-/y}$ versus wild-type mice. Consistent with elevated dendritic I_h, voltage sag, rebound, and resonance frequency were significantly higher and temporal summation was lower in the dendrites of *fmr1*$^{-/y}$ mice. Dendritic expression of the h-channel subunit HCN1, but not HCN2, was higher in the CA1 region of *fmr1*$^{-/y}$ mice. Interestingly, whereas mGluR-mediated persistent decreases in I_h occurred in both wild-type and *fmr1*$^{-/y}$ mice, persistent increases in I_h that occurred after LTP induction in wild-type mice were absent in *fmr1*$^{-/y}$ mice. Thus, chronic upregulation of dendritic I_h in conjunction with impairment of homeostatic h-channel plasticity represents a dendritic channelopathy in this model of mental retardation and may provide a mechanism for the cognitive impairment associated with FXS.

INTRODUCTION

Fragile X syndrome (FXS) is the most common form of inherited mental retardation with a variety of phenotypes including impaired cognitive ability, problems with working memory, autistic behavior, and increased incidence of epilepsy. FXS is characterized by the absence of the RNA-binding protein fragile X mental retardation protein (FMRP) (Bell et al., 1991). Mice lacking FMRP, such as the *fmr1* knockout (*fmr1*$^{-/y}$) mouse, perform poorly in hippocampal-dependent spatial learning tasks (Bakker et al., 1994). Interestingly, the performance of *fmr1*$^{-/y}$ mice was similar to mice lacking proteins involved in long-term potentiation (LTP), a proposed cellular correlate of learning (e.g., Silva et al., 1992).

Several FMRP-target mRNAs are localized in neuronal dendrites and encode for voltage-gated channels or proteins involved in the regulation of channel expression and/or function (Darnell et al., 2011; Bassell and Warren, 2008). Incorrect gene expression, channel function, and/or loss of posttranslational channel regulation can have substantial effects on the control of cellular excitability. The physiological regulation of cellular excitability and dendritic integration through plasticity of voltage-gated ion channels is hypothesized to maintain the input-output characteristics of a neuron within normal limits (Turrigiano and Nelson, 2000). However, changes in dendritic channels in neurological disorders or disease can also alter the input-output relationship and result in a pathophysiological state (Bernard et al., 2004; Jung et al., 2007). One channel that undergoes activity-dependent plasticity and is altered in neurological disease is the h-channel (van Welie et al., 2004; Brager and Johnston, 2007; Fan et al., 2005; Jung et al., 2007; Shin et al., 2008).

h-channels are widely distributed in the central nervous system. In the hippocampus, h-channels are composed primarily of HCN1 and HCN2 subunits (Santoro et al., 2000). In CA1 pyramidal neurons the density of h-channels increases with distance from the soma along the apical dendrite (Magee, 1998). The high density of h-channels in the dendrites allows I_h (the current mediated by h-channels) to significantly contribute to the total membrane conductance and thereby exert strong influence over neuronal function in the subthreshold voltage range near rest. Subtle modifications in the physiology of h-channels can produce significant changes in synaptic integration and neuronal excitability (Santoro et al., 2000; Magee, 1999; Poolos et al., 2002).

Using whole-cell recording from CA1 pyramidal neuron apical dendrites, we show that dendritic physiology in the *fmr1*$^{-/y}$ mouse is altered in a manner consistent with elevated dendritic I_h. Differences in hippocampal HCN1 protein expression were consistent with our physiological results. Interestingly, activity-dependent increases in I_h following LTP induction were absent in *fmr1*$^{-/y}$ mice. Elevated dendritic expression of I_h coupled with impaired h-channel plasticity might thus indicate some of the cellular mechanisms underlying the cognitive impairments associated with FXS.

RESULTS

Dendritic Properties of *fmr1*$^{-/y}$ Mice Are Significantly Different from Wild-Type

The intrinsic properties of hippocampal pyramidal neurons, established in part by the contribution of dendritic voltage-gated

ion channels, strongly influence the manner in which synaptic inputs are combined and propagated from the dendrites to the soma. In particular a proportion of the total population of h-channels is active at rest and contributes to the resting membrane potential (V_m), input resistance (R_N), and membrane time constant (τ_m) of CA1 neurons (Magee, 1998). We used somatic and dendritic whole-cell recording to test whether there were significant differences in the V_m, R_N, and τ_m of CA1 neurons between *fmr1*$^{-/y}$ and wild-type (WT) mice. We found that V_m was significantly more depolarized, R_N was lower, and τ_m was faster, in the dendrites versus the soma for both WT and *fmr1*$^{-/y}$ mice; consistent with a higher density of h-channels in the apical dendrite. There were no significant differences between WT and *fmr1*$^{-/y}$ mice using somatic recordings (see Figure S1 available online). When we compared the dendrites between *fmr1*$^{-/y}$ and WT mice, however, we found that the dendritic V_m of *fmr1*$^{-/y}$ mice was significantly depolarized versus WT (knockout [ko], -61 ± 0.6mV; WT, -64 ± 0.6mV; $p < 0.05$). Furthermore, dendritic R_N was significantly lower (Figures 1A–1C) and dendritic τ_m was significantly faster (WT, 17 ± 2 ms; ko, 8 ± 1 ms; $p < 0.05$) in *fmr1*$^{-/y}$ mice versus WT.

To test the hypothesis that the differences in dendritic properties were due to elevated I_h, we took advantage of several unique characteristics of h-channels and measured electrophysiological parameters that are sensitive to the amount of I_h (Brager and Johnston, 2007). Voltage sag (sag) during step current injections can be due to the relatively slow activation/deactivation kinetics I_h (Magee, 1998). We found that dendritic sag from hyperpolarizing current steps was 38% higher in *fmr1*$^{-/y}$ mice versus WT (Figures 1D–1F). Rebound amplitude following a hyperpolarization is due in part to the slow closing of h-channels. The amount of rebound from a given steady-state hyperpolarization is increased with larger I_h (Brager and Johnston, 2007). Dendritic rebound was 43% higher in *fmr1*$^{-/y}$ mice versus WT (Figures 1G–1I). The same kinetic properties that underlie sag and rebound allow I_h to act as a resonator conductance, and differences in resonance frequency (f_R) reflect differences in I_h (Hutcheon and Yarom, 2000; Narayanan and Johnston, 2007). Similar to sag and rebound, dendritic f_R was 42% higher in *fmr1*$^{-/y}$ mice versus WT (Figures 1J–1L). I_h reduces temporal summation by repolarizing the membrane during an excitatory postsynaptic potential (EPSP) (Magee, 1998). Consistent with elevated I_h, we found that dendritic temporal summation was significantly lower in *fmr1*$^{-/y}$ mice versus WT (Figures 1M–1O). When measured from the soma, we found no significant difference in sag, rebound, f_R, or summation between WT and *fmr1*$^{-/y}$ mice (Figure S1).

As a further test of the contribution of I_h to the differences in dendritic properties, we compared WT and *fmr1*$^{-/y}$ dendritic recordings before and after application of the h-channel blocker ZD7288. Extracellular application of 20 μM ZD7288 significantly increased R_N in both WT and *fmr1*$^{-/y}$ dendrites (Figure 1C). Furthermore, block of I_h significantly decreased sag, rebound, and f_R and increased temporal summation in both WT and *fmr1*$^{-/y}$ dendrites (Figures 1F, 1I, 1L, and 1O). After block of I_h by ZD7288, dendritic properties were no longer significantly different between WT and *fmr1*$^{-/y}$ dendrites. These electrophysiological results suggest that dendritic, but not somatic, I_h is significantly higher in *fmr1*$^{-/y}$ mice.

Elevated HCN1 Levels in the CA1 Region of the *fmr1*$^{-/y}$ Mouse Hippocampus

Our electrophysiological data support the hypothesis that I_h is higher in the dendrites of CA1 neurons from *fmr1*$^{-/y}$ mice versus WT mice. We sought to further test this hypothesis by examining h-channel proteins using immunohistochemistry and western blotting. We used antibodies to label the h-channel subunits HCN1 and HCN2. As expected, the intensity of HCN1 and HCN2 labeling increased with distance from the cell body layer indicative of the h-channel gradient. Measuring the intensity along a line perpendicular to, but not including, the pyramidal cell body layer in CA1 allows for a comparison of the distribution of HCN1 and HCN2 staining between slices (Shin et al., 2008). We found that the intensity of the HCN1 fluorescence, but not HCN2, was higher in the distal dendrites of *fmr1*$^{-/y}$ mice versus WT mice (Figures 2A–2F). The difference in HCN1 staining between *fmr1*$^{-/y}$ and WT mice persisted when the HCN1 signal was normalized to dendritic marker MAP2 (Figure S2). We used western blot analysis to determine if there was higher HCN protein levels in the dendritic field of the CA1 region of the *fmr1*$^{-/y}$ mouse versus WT. We found that HCN1, but not HCN2, protein levels were significantly higher in homogenates from the dendritic region of CA1 in *fmr1*$^{-/y}$ versus WT (Figures 2G and 2H). These results suggest that the higher dendritic I_h in *fmr1*$^{-/y}$ mice is due in part to an increase in the distal dendritic expression of the h-channel subunit HCN1.

Intrinsic Plasticity Is Impaired in *fmr1*$^{-/y}$ Mice

Homeostatic mechanisms that maintain neuronal output are essential for the stabilization of neural networks during classical Hebbian synaptic plasticity (Turrigiano, 2011). We previously demonstrated that activation of group I metabotropic glutamate receptors (mGluRs) results in long-term depression (LTD) and an accompanying decrease of I_h in CA1 neurons (Brager and Johnston, 2007). In the hippocampus of *fmr1*$^{-/y}$ mice, group I mGluR-dependent LTD is enhanced, whereas NMDA receptor-dependent LTD is unaffected (Huber et al., 2002). To test whether mGluR-dependent h-channel plasticity is altered in *fmr1*$^{-/y}$ mice, we measured intrinsic properties before and after activation of group I mGluRs (100 μM DHPG for 10 min). Application of DHPG to either WT or *fmr1*$^{-/y}$ CA1 neurons produced a transient depolarization that recovered by 30 min after wash (Figure 3A). This transient activation of mGluRs decreased EPSP slope by 23% in WT and 40% in *fmr1*$^{-/y}$ mice 30 min after DHPG application (Figures 3B and 3C). In agreement with our previous observations in rat hippocampus (Brager and Johnston, 2007), we found that mGluR activation significantly increased R_N by 85% in WT mice and by 83% in *fmr1*$^{-/y}$ mice (Figure 3D). Consistent with a decrease in I_h, f_R, rebound, and sag were significantly decreased after DHPG application in WT, and f_R and rebound were significantly decreased in *fmr1*$^{-/y}$ mice (Figures 3E–3G). Based on these results, we conclude that mGluR-dependent plasticity of I_h occurs in both WT and *fmr1*$^{-/y}$ mice.

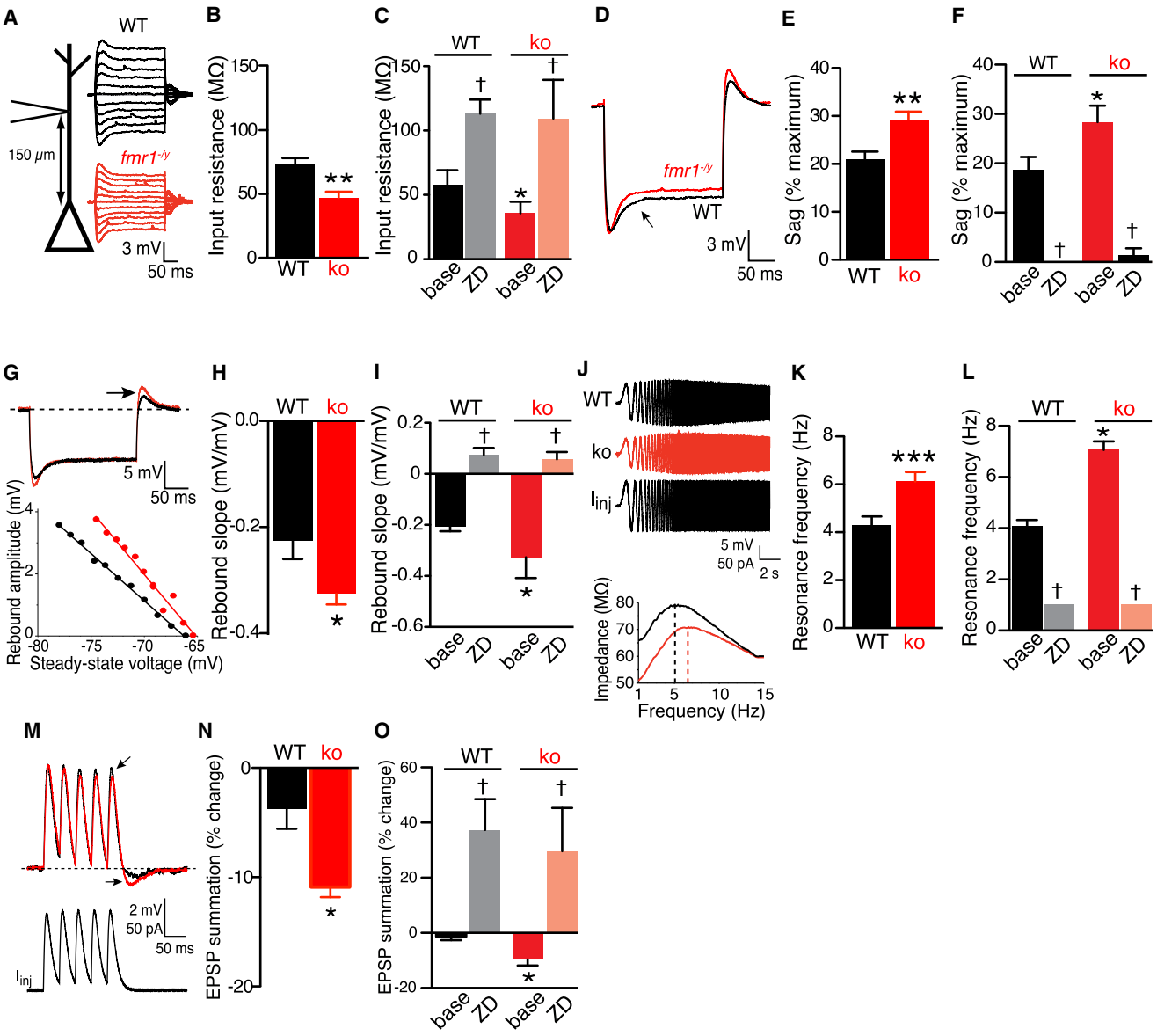

Figure 1. h-Channel Dependent Dendritic Properties Are Significantly Different between WT and *fmr1*$^{-/y}$ Mice

(A) Diagram of recording locations and representative dendritic recordings from WT and *fmr1*$^{-/y}$ mice.

(B) Group data showing that dendritic R_N was significantly lower in *fmr1*$^{-/y}$ mice (n = 6) versus WT (n = 6).

(C) Group data showing that application of ZD significantly increased R_N in both WT (n = 4) and *fmr1*$^{-/y}$ mice (n = 4).

(D) Representative dendritic whole-cell recordings showing that there was more sag (arrow) in the dendrites of *fmr1*$^{-/y}$ mice versus WT.

(E) Group data showing that dendritic sag was significantly higher in *fmr1*$^{-/y}$ mice.

(F) Group data showing that application of ZD significantly decreased sag in both WT and *fmr1*$^{-/y}$ mice.

(G) Representative dendritic whole-cell recordings (left) and plot used to calculate rebound slope (right) from WT and *fmr1*$^{-/y}$ mice.

(H) Group data showing that dendritic rebound slope was significantly higher in *fmr1*$^{-/y}$ mice.

(I) Group data showing that application of ZD significantly decreased rebound in both WT and *fmr1*$^{-/y}$ mice.

(J) Representative voltage traces and ZAP used to determine f_R (dashed line). Note the rightward shift in the *fmr1*$^{-/y}$ (red) versus the WT (black).

(K) Group data showing that dendritic f_R was significantly higher in *fmr1*$^{-/y}$ mice.

(L) Group data showing that application of ZD significantly decreases f_R in both WT and *fmr1*$^{-/y}$ mice.

(M) Representative traces used to measure temporal summation of *fmr1*$^{-/y}$ mice versus WT.

(N) Group data showing that dendritic temporal summation was significantly less in *fmr1*$^{-/y}$ mice.

(O) Group data showing that application of ZD significantly increased dendritic summation in both WT and *fmr1*$^{-/y}$ mice.

Group data are presented as mean ± SEM. *p < 0.05; **p < 0.01; ***p < 0.005 significantly different from WT. †p < 0.05 significantly different from baseline.

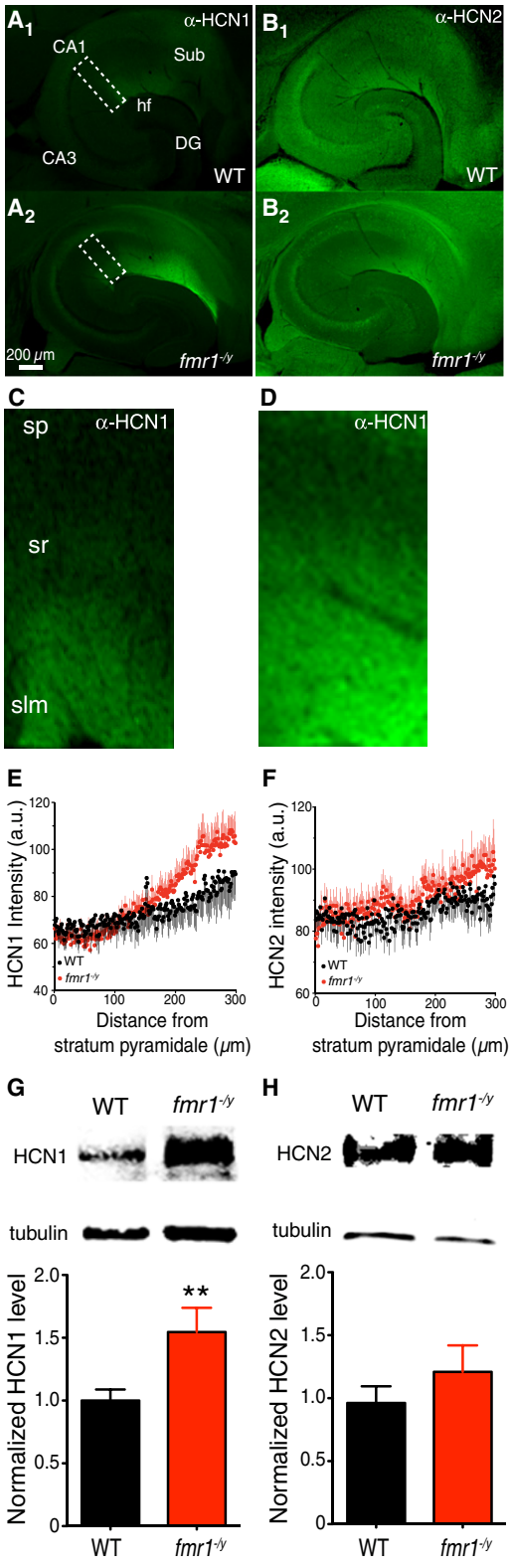

Figure 2. Distal Dendritic HCN1 Expression in Area CA1 Is Higher in *fmr1*$^{-/y}$ Mice

(A) Representative fluorescent images showing HCN1 staining from a WT (A_1) and an *fmr1*$^{-/y}$ (A_2) mouse section (Sub, subiculum; hf, hippocampal fissure; DG, dentate gyrus). Fluorescent intensity was measured along the dashed line.

(B) Representative fluorescent images showing HCN2 staining from a WT (B_1) and an *fmr1*$^{-/y}$ (B_2) mouse section.

(C and D) Region indicated by the box in (A_1) and (A_2). sp, stratum pyramidale; sr, stratum radiatum; slm, stratum lacunosum-moleculare.

(E) A plot of intensity as a function of location showing that distal dendritic HCN1 staining was higher in *fmr1*$^{-/y}$ mice versus WT mice.

(F) Intensity profile showing that there was no difference in HCN2 staining between *fmr1*$^{-/y}$ and WT mice.

(G) The total amount of HCN1 protein in the CA1 region of the *fmr1*$^{-/y}$ hippocampus was significantly higher than WT.

(H) Representative western blot from WT and *fmr1*$^{-/y}$ mice for HCN2 and tubulin. There was no significant difference in the total amount of HCN2 protein between *fmr1*$^{-/y}$ and WT hippocampus.

Group data are presented as mean ± SEM.**$p < 0.01$.

In CA1 neurons, theta-burst firing of action potentials paired with EPSPs (theta-burst pairing, TBP) results in an NMDA-dependent increase in I_h (Fan et al., 2005). To test whether the higher dendritic I_h in *fmr1*$^{-/y}$ mice occludes the TBP-dependent increases in I_h, we induced TBP-LTP in CA1 neurons from both WT and *fmr1*$^{-/y}$ mice. CA1 neurons from both WT and *fmr1*$^{-/y}$ mice displayed a significant increase in EPSP slope following TBP (Figures 4A and 4B). In agreement with previous studies (Fan et al., 2005; Narayanan and Johnston, 2007), TBP was accompanied by a significant decrease in R_N in WT mice (baseline, 82 ± 7 MΩ; TBP, 68 ± 6 MΩ; n = 5, $p < 0.05$) (Figures 4C and 4D). Interestingly, there was no significant change in R_N in *fmr1*$^{-/y}$ mice. Consistent with an increase in I_h, TBP significantly increased f_R, rebound, and sag in WT mice (Figures 4E–4G). In contrast, there was no significant change in f_R, rebound, or sag in *fmr1*$^{-/y}$ neurons after TBP. We thus conclude that the activity-dependent expression of I_h plasticity that normally occurs following TBP-LTP is absent in *fmr1*$^{-/y}$ mice.

DISCUSSION

Neurons from patients and animal models of FXS show significant morphological and synaptic alterations. Here, we show that a significant change to the intrinsic properties of the dendrites of CA1 neurons occurs in the *fmr1*$^{-/y}$ mouse model of FXS. Electrophysiological data support the hypothesis that these changes are due in part to a dendritic enhancement of the hyperpolarization-activated nonselective cationic current, I_h, in the distal dendrites. Furthermore, this elevation in I_h appears to be due to increased distal dendritic expression of the HCN1 subunit. Interestingly, activity-dependent increases in I_h are absent, whereas activity-dependent decreases in I_h remain. These data represent the first physiological description of a channelopathy involving dendritic h-channels associated with FXS.

Impact on Dendritic Function

I_h plays a complex role in controlling membrane excitability. What is the impact of elevated I_h in FXS on dendritic function? Elevated I_h will reduce dendritic excitability by decreasing R_N as well as reducing temporal and spatial summation of subthreshold EPSPs. I_h also constrains distal dendritic spikes

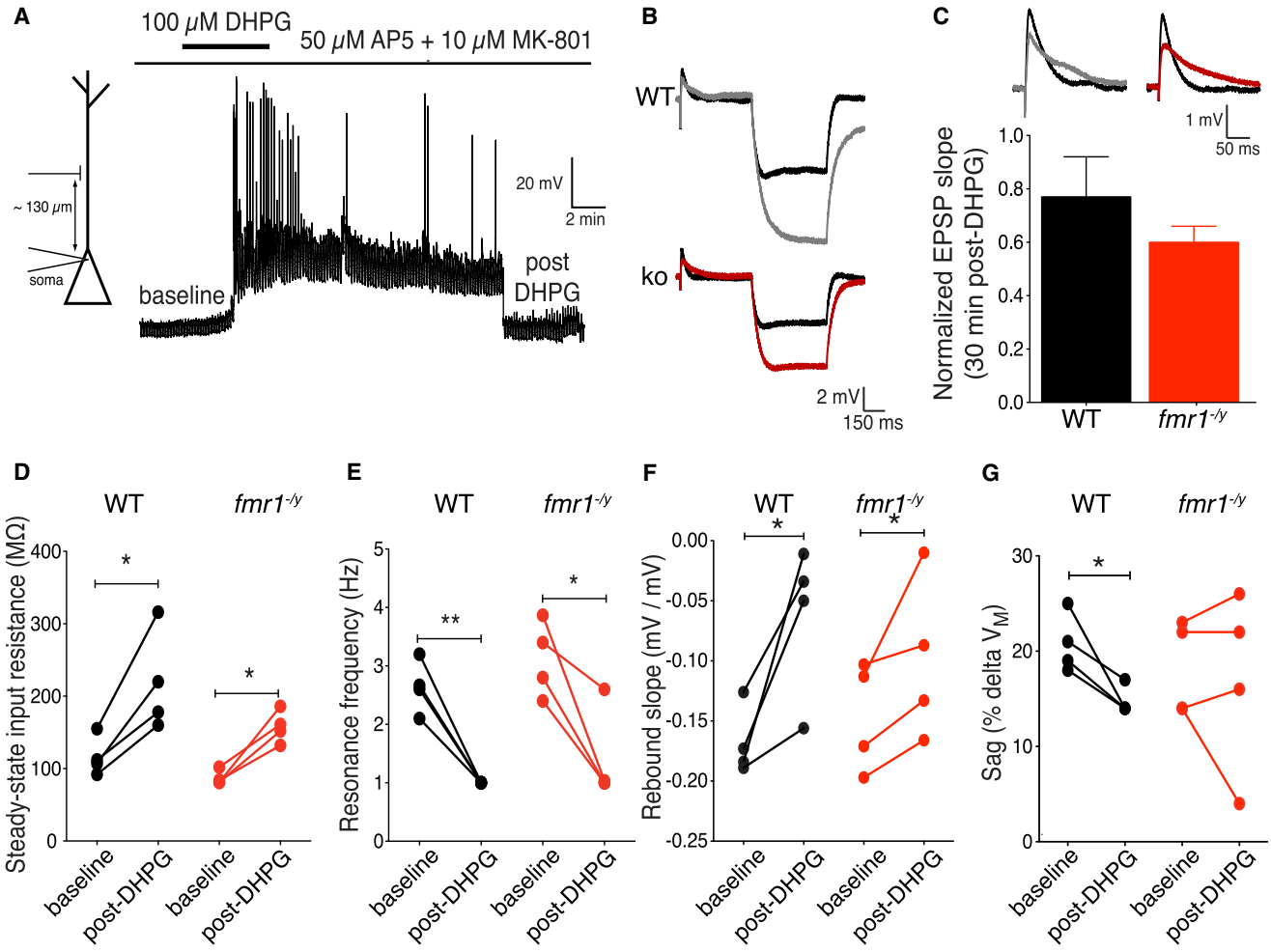

Figure 3. mGluR-Dependent Plasticity Is Present in Both WT and *fmr1*$^{-/y}$ Mice

(A) Time course of membrane potential change following a 10 min DHPG application.

(B) Representative traces from WT and *fmr1*$^{-/y}$ mice before and after DHPG application showing LTD of EPSPs and increased R_N.

(C) Group data showing the normalized decrease in EPSP slope 30 min after DHPG washout for both WT (n = 4) and *fmr1*$^{-/y}$ mice (n = 4). Inset shows expanded time scale of traces in (B).

(D) Group data showing that R_N significantly increased after DHPG washout in both WT and *fmr1*$^{-/y}$ mice.

(E) Group data showing that f_R significantly decreased after DHPG washout in both WT and *fmr1*$^{-/y}$ mice.

(F) Group data showing that rebound slope significantly decreased after DHPG washout in both WT and *fmr1*$^{-/y}$ mice.

(G) Group data showing that sag significantly decreased after DHPG washout in WT but not *fmr1*$^{-/y}$ mice.

Group data are presented as mean ± SEM.*p < 0.05; **p < 0.01.

by increasing inactivation of both T- and N-type Ca^{2+} channels (Tsay et al., 2007). The normal gradient of h-channels regulates the propagation of signals between the dendrites and the soma, and changes in the amount of dendritic I_h will strongly influence somato-dendritic coupling (Magee, 1998, 1999; Poolos et al., 2002). The increase in dendritic I_h in FXS would decrease somato-dendritic coupling, reducing the likelihood of synaptic inputs eliciting an action potential at the soma.

Elevated I_h will not only have inhibitory influences on dendritic excitability but also increase membrane excitability by depolarizing the membrane potential closer to the threshold for dendritic spike initiation and by augmenting the depolarizing rebound potential that occurs following a hyperpolarization. We found that rebound from hyperpolarization was higher in the dendrites of *fmr1*$^{-/y}$ mice. This increase in rebound either alone (Chen et al., 1999) or in concert with the activation of low-threshold voltage-dependent calcium channels could elicit a dendritic spike or dendritic plateau potential (Berger et al., 2003; Tsay et al., 2007). There is a high density of GABAergic synapses and $GABA_B$ receptors in the distal dendrites of CA1 neurons (Otmakhova and Lisman, 2004). It is, therefore, possible that in *fmr1*$^{-/y}$ mice the normal inhibitory input into the distal dendrites of CA1 neurons will in fact result in significant dendritic excitation.

These two opposing actions of elevated I_h on cellular excitability will have the complicated impact of decreasing R_N,

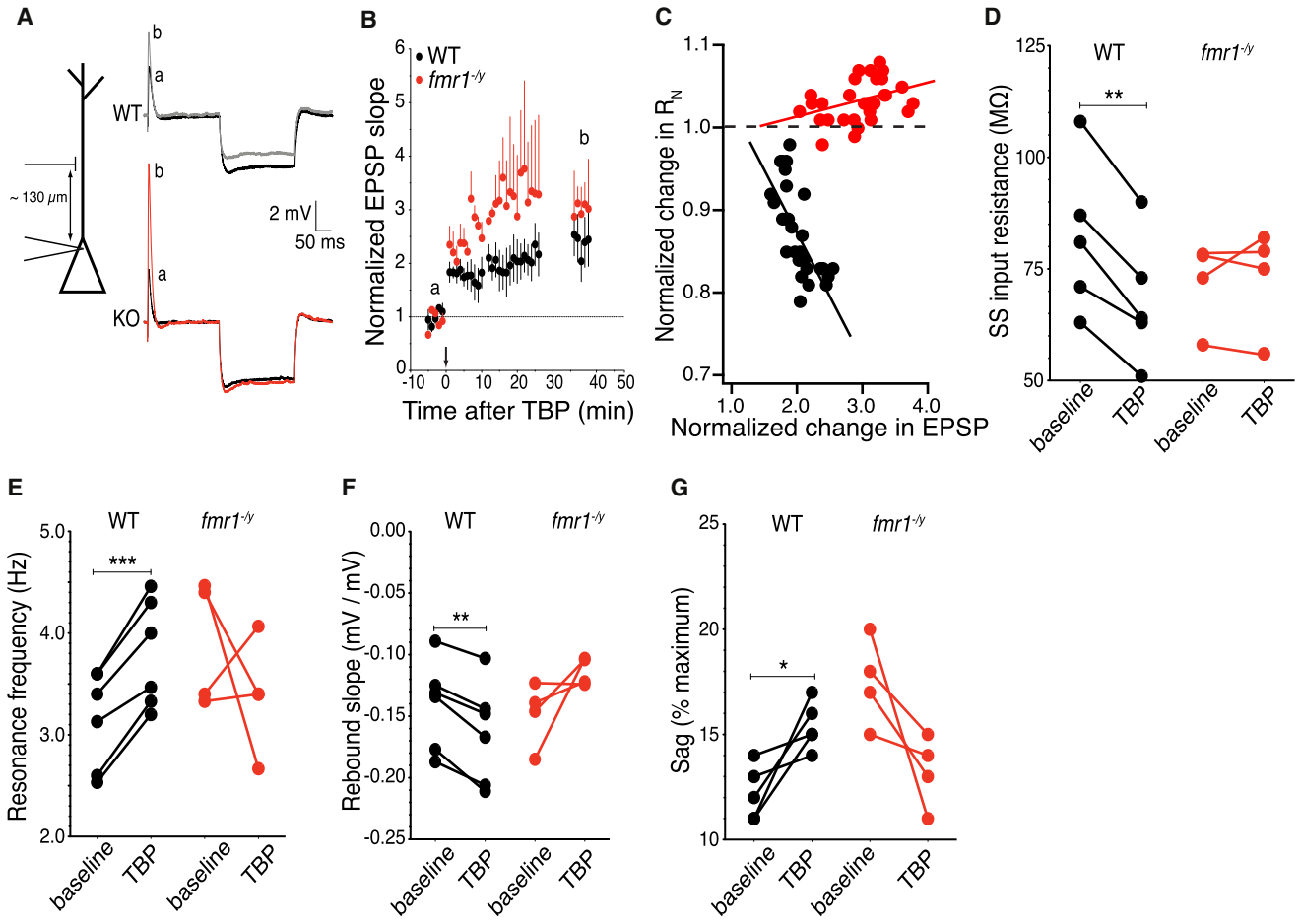

Figure 4. TBP-Dependent I_h Plasticity Is Absent in *fmr1*$^{-/y}$ Mice

(A) Representative traces (from time points indicated by a and b in B) from WT (black) and *fmr1*$^{-/y}$ (red) mice before and after TBP showing LTP of EPSPs and decreased R_N.

(B) The time course of EPSP slope change after TBP for WT (n = 6) and *fmr1*$^{-/y}$ mice (n = 4).

(C) The time course of RN change after TBP for WT (n = 6) and *fmr1*$^{-/y}$ mice (n = 4).

(D) Group data showing that R_N significantly decreased after TBP in WT but not *fmr1*$^{-/y}$ mice.

(E) Group data showing that f_R significantly increased after TBP in WT but not *fmr1*$^{-/y}$ mice.

(F) Group data showing that rebound slope significantly increased after TBP in WT but not *fmr1*$^{-/y}$ mice.

(G) Group data showing that sag significantly increased after TBP in WT but not *fmr1*$^{-/y}$ mice.

Group data are presented as mean ± SEM.*p < 0.05; **p < 0.01; ***p < 0.005.

temporal and spatial summation, and somato-dendritic coupling, making it harder for synaptic inputs to summate and elicit a somatic action potential, whereas also increasing the likelihood of local dendritic regenerative events. The exact impact of elevated dendritic I_h on information processing in FXS requires further investigation.

I_h Plasticity in FXS

Transient and persistent changes in I_h, which alters neuronal intrinsic excitability, occur during and after induction of synaptic plasticity (Brager and Johnston, 2007; Fan et al., 2005). This coordinated change in synaptic and intrinsic excitability is not completely understood, but one current hypothesis is that intrinsic plasticity can alleviate the inherent instability of synaptic plasticity. Following induction of LTP there is a persistent increase in I_h throughout the dendrites of CA1 neurons (Fan et al., 2005; Narayanan and Johnston, 2007). We found that although TBP-dependent LTP was not different between WT and *fmr1*$^{-/y}$ mice, I_h plasticity was absent in the latter. One possibility is that changes in the intracellular signaling molecules occlude any increase in I_h after TBP-LTP. For example, CAMKII levels are elevated in *fmr1*$^{-/y}$ mice (Zalfa et al., 2003), and the activation of CAMKII is required for TBP-dependent I_h plasticity (Fan et al., 2005). It is possible that the already higher levels of CAMKII lead to elevated dendritic I_h and that TBP-LTP is unable to further increase in I_h in *fmr1*$^{-/y}$ mice. The concomitant increase in I_h that normally occurs with LTP is believed to be one mechanism by which homeostatic regulation of neural network stability can be achieved (Narayanan and Johnston, 2007). Our results suggest that despite the appearance of normal

synaptic potentiation, the deficit in intrinsic plasticity may lead to inherent network destabilization. The combined plasticity of I_h and synaptic strength results in preferential tuning of the dendrites to selected synaptic inputs. This form of homeostatic plasticity is believed to be critical for information storage and processing by neuronal networks (Turrigiano and Nelson, 2000). A loss of normal h-channel plasticity, with or without accompanying deficits in synaptic plasticity, could have profound effects on neuronal signal processing.

Potential Mechanisms

How does the absence of FMRP lead to an increase in dendritic I_h and HCN1 protein? FMRP may bind to and regulate the translation of HCN1 mRNA. Classically, FMRP acts as a translational repressor (but see Gross et al., 2011). If HCN1 mRNA is a target of FMRP, then the loss of FMRP will directly result in elevated HCN1 expression. Indeed, our data show that expression of HCN1 protein is higher in the CA1 region of the *fmr1*$^{-/y}$ mouse hippocampus. FMRP may also interact directly with ion channel proteins. In the olfactory bulb and brain stem, FMRP can bind to and regulate the gating of the sodium-activated potassium channel, Slack (Brown et al., 2010). FMRP may bind directly to h-channel proteins or regulate the binding between HCN subunits and auxiliary proteins such as tetratricopeptide repeat-containing Rab8b-interacting protein (TRIP8b) (Santoro et al., 2004). The interaction between TRIP8b and HCN subunits regulates both the gating and surface expression of h-channels.

The elevated I_h may also be a compensatory change due to the loss of FMRP-dependent regulation of another protein. FMRP is necessary for normal synapse elimination during development (Pfeiffer and Huber, 2007). One possibility is that excessive synaptic excitation may lead to a homeostatic increase in I_h. Upregulation of hippocampal h-channels can occur following high levels of AMPA receptor activation (van Welie et al., 2004). Increased excitatory input from CA3 Schaeffer collaterals due to elevated neurotransmitter release (Deng et al., 2011) could lead to excess CA1 AMPA receptor activation in *fmr1*$^{-/y}$ mice. Additionally, synaptic inputs from layer III of the entorhinal cortex (EC) onto the distal dendrites of CA1 neurons regulate the normal h-channel gradient (Shin and Chetkovich, 2007). Increased excitatory input from the EC, due to improper synaptic pruning, could lead to a compensatory increase in I_h. Alternatively, elevated I_h may be in response to loss of another ion channel. Invertebrate studies suggest that there may be homeostatic coregulation of I_h and I_A including functional reciprocity (Harris-Warrick et al., 1995). There are conflicting reports about Kv4.2 expression, the putative subunit of I_A, in the *fmr1*$^{-/y}$ hippocampus. One study reported that FMRP promotes translation of Kv4.2 mRNA and that Kv4.2 protein levels are reduced in *fmr1*$^{-/y}$ mice (Gross et al., 2011). More recently, a second study reported that FMRP acts as a translational repressor and that Kv4.2 expression is higher in the *fmr1*$^{-/y}$ hippocampus compared to WT (Lee et al., 2011). It is possible that changes in Kv4.2 expression results in a compensatory increase in I_h, in part by increased HCN1 expression. We are currently investigating these hypotheses as potential mechanisms underlying the change in dendritic function in FXS.

In summary we found that the dendrites of CA1 neurons from *fmr1*$^{-/y}$ mice have altered intrinsic properties consistent with an elevation of I_h. This elevation is due in part to the increased distal dendritic expression of the h-channel subunit HCN1. Furthermore, this elevation in dendritic I_h appears to occlude normal homeostatic intrinsic plasticity of I_h that occurs during LTP. These results suggest that altered dendritic processing and the potential for network instability may underlie some of the neurological deficits associated with FXS.

EXPERIMENTAL PROCEDURES

Acute Hippocampal Slices and Electrophysiology

All experiments were conducted in accordance with the University's IACUC. Hippocampal slices (300 μm) were prepared from 2- to 3-month-old male WT and *fmr1*$^{-/y}$ mice (C57BL/6) as described previously (Fan et al., 2005) (see Extended Experimental Procedures). Slices were placed in a holding chamber filled with ACSF containing (125 NaCl, 2.5 KCl, 1.25 NaH_2PO_4, 25 $NaHCO_3$, 2 $CaCl_2$, 2 $MgCl_2$, and 12.5 dextrose, bubbled continuously with 95% O_2/5% CO_2) warmed to 35°C for 30 min and then kept at RT. Hippocampal slices were placed into a submerged recording chamber and perfused with ACSF (as above except 3.0 KCl and 1.0 $MgCl_2$) at 31°C–33°C and viewed with a Zeiss Axioskop. For physiological measurements (Figure 1), 10 μM DNQX, 50 μM AP5, 2 μM SR95531, and 5 μM CGP52432 were present throughout. For mGluRs experiments (Figure 3), AP5 and 10 μM MK-801 were included in the ACSF (Brager and Johnston, 2007). For LTP experiments (Figure 4), $GABA_A$- and $GABA_B$-mediated IPSPs were blocked by SR95531 and CGP55845, and area CA3 was removed. All drugs were made from stock solutions in water or DMSO (final concentration of DMSO ≤0.1%). Drugs were obtained from Ascent Scientific (Bristol, UK).

Pipettes (4–6 MΩ) were pulled from borosilicate glass and filled with solution containing 120 mM K-gluconate, 20 mM KCl, 10 mM HEPES, 4 mM NaCl, 4 mM MgATP, 0.3 mM Na-GTP, and 7 mM K_2-phosphocreatine (pH 7.3). Series resistance (R_S) was monitored throughout the recording, and experiments with R_S >30 MΩ were discarded. EPSPs of 4–6mV were elicited using tungsten-stimulating electrodes placed <20 μm from the apical dendrite ~100–150 μm from the soma. Action potentials were elicited by current injection into the soma (1–2 nA for 2 ms).

Data were sampled at 20 kHz, filtered at 3 kHz, and digitized by an ITC-18 interface. EPSPs were quantified by linear fit to the initial slope. H-sensitive parameters were measured and analyzed as described in the Extended Experimental Procedures.

Immunohistochemistry

Two to 3-month-old male *fmr1*$^{-/y}$ and WT mice were anesthetized and perfusion fixed 4% paraformaldehyde (PFA) at 4°C. The brain was removed, post-fixed in PFA for 2 hr at RT, and placed in 30% sucrose in PBS overnight at 4°C. A total of 50 μm near-horizontal thin sections containing the hippocampus were cut on a freezing microtome. Slices were washed and then incubated in a blocking buffer solution containing 5% Normal Goat Serum, 0.1% Triton X-100, and PBS (PBS-T), and then incubated in primary antibody (1:2,000 concentration in PBS-T) against either HCN1 or HCN2 overnight at 4°C. Sections were then washed with PBS then placed in PBS-T containing a secondary antibody overnight at 4°C. The slices were then washed in PBS and mounted on microscope slides. The sections were visualized on a fluorescent microscope; images were captured by CCD camera, and analyzed using ImageJ (National Institutes of Health). The intensity of staining was quantified by measuring the pixel intensity along a line perpendicular to the cell body axis in CA1 (Shin et al., 2008).

Western Blotting

Area CA1 was isolated from three to five individual hippocampal slices frozen on dry ice. Tissue was homogenized in lysis buffer containing protease inhibitors. Homogenates were centrifuged at 80 × *g* for 10 min, resolved using SDS-PAGE, and transferred to nitrocellulose membranes. Membranes were

blocked in blocking buffer (LI-COR) overnight at 4°C or for 1 hr at RT. Membranes were incubated for 2 hr at RT or overnight at 4°C in primary antibodies diluted in blocking buffer (gp α-HCN1, 1:2,000; gp α-HCN2, 1:2,000; mouse α-tubulin 1:20,000). Membranes were washed in PBS plus 0.05% Tween 20 (PBS+) and then incubated in species-appropriate secondary in PBS+ for 45 min at RT. Membranes were then washed in PBS+ followed by PBS and visualized on an Odyssey imaging system (LI-COR). Blots were analyzed using ImageJ. HCN protein levels were normalized to tubulin levels as a control for protein loading. Homogenates from four *fmr1*$^{-/y}$ and four WT mice were used for four separate western blots.

SUPPLEMENTAL INFORMATION

Supplemental Information includes Extended Experimental Procedures and two figures and can be found with this article online at doi:10.1016/j.celrep.2012.02.002.

LICENSING INFORMATION

ACKNOWLEDGMENTS

The authors thank Dr. Kimberly Huber for providing the founder *fmr1*$^{-/y}$ mice; Dr. Dane Chetkovich for the HCN1 and HCN2 antibodies; and Drs. Kimberly Raab-Graham, Kelly Dougherty, Nikolai Dembrow, Raymond Chitwood, and Jennifer Siegel for helpful discussions and comments on the manuscript. This work was supported by grants from FRAXA (to D.H.B.), The University of Texas Austin Undergraduate Research Fellowship (to A.R.A.), and the National Institutes of Health Grant MH048432 (to D.J.).

Received: June 25, 2011
Revised: December 27, 2011
Accepted: February 1, 2012
Published online: March 15, 2012

REFERENCES

Bakker, C.E., Verheij, C., Willemsen, R., van der Helm, R., Oerlemans, F., Vermey, M., Bygrave, A., Hoogeveen, A.T., and Oostra, B.A. (1994). Fmr1 knockout mice: A model to study fragile X mental retardation. Cell *78*, 23–33.

Bassell, G.J., and Warren, S.T. (2008). Fragile X syndrome: loss of local mRNA regulation alters synaptic development and function. Neuron *60*, 201–214.

Bell, M.V., Hirst, M.C., Nakahori, Y., MacKinnon, R.N., Roche, A., Flint, T.J., Jacobs, P.A., Tommerup, N., Tranebjaerg, L., Froster-Iskenius, U., et al. (1991). Physical mapping across the fragile X: hypermethylation and clinical expression of the fragile X syndrome. Cell *64*, 861–866.

Berger, T., Senn, W., and Lüscher, H.-R. (2003). Hyperpolarization-activated current Ih disconnects somatic and dendritic spike initiation zones in layer V pyramidal neurons. J. Neurophysiol. *90*, 2428–2437.

Bernard, C., Anderson, A., Becker, A., Poolos, N.P., Beck, H., and Johnston, D. (2004). Acquired dendritic channelopathy in temporal lobe epilepsy. Science *305*, 532–535.

Brager, D.H., and Johnston, D. (2007). Plasticity of intrinsic excitability during long-term depression is mediated through mGluR-dependent changes in I(h) in hippocampal CA1 pyramidal neurons. J. Neurosci. *27*, 13926–13937.

Brown, M.R., Kronengold, J., Gazula, V.R., Chen, Y., Strumbos, J.G., Sigworth, F.J., Navaratnam, D., and Kaczmarek, L.K. (2010). Fragile X mental retardation protein controls gating of the sodium-activated potassium channel Slack. Nat. Neurosci. *13*, 819–821.

Chen, K., Baram, T.Z., and Soltesz, I. (1999). Febrile seizures in the developing brain result in persistent modification of neuronal excitability in limbic circuits. Nat. Med. *5*, 888–894.

Darnell, J.C., Van Driesche, S.J., Zhang, C., Hung, K.Y.S., Mele, A., Fraser, C.E., Stone, E.F., Chen, C., Fak, J.J., Chi, S.W., et al. (2011). FMRP stalls ribosomal translocation on mRNAs linked to synaptic function and autism. Cell *146*, 247–261.

Deng, P.Y., Sojka, D., and Klyachko, V.A. (2011). Abnormal presynaptic short-term plasticity and information processing in a mouse model of fragile X syndrome. J. Neurosci. *31*, 10971–10982.

Fan, Y., Fricker, D., Brager, D.H., Chen, X., Lu, H.-C., Chitwood, R.A., and Johnston, D. (2005). Activity-dependent decrease of excitability in rat hippocampal neurons through increases in I(h). Nat. Neurosci. *8*, 1542–1551.

Gross, C., Yao, X., Pong, D.L., Jeromin, A., and Bassell, G.J. (2011). Fragile X mental retardation protein regulates protein expression and mRNA translation of the potassium channel Kv4.2. J. Neurosci. *31*, 5693–5698.

Harris-Warrick, R.M., Coniglio, L.M., Levini, R.M., Gueron, S., and Guckenheimer, J. (1995). Dopamine modulation of two subthreshold currents produces phase shifts in activity of an identified motoneuron. J. Neurophysiol. *74*, 1404–1420.

Huber, K.M., Gallagher, S.M., Warren, S.T., and Bear, M.F. (2002). Altered synaptic plasticity in a mouse model of fragile X mental retardation. Proc. Natl. Acad. Sci. USA *99*, 7746–7750.

Hutcheon, B., and Yarom, Y. (2000). Resonance, oscillation and the intrinsic frequency preferences of neurons. Trends Neurosci. *23*, 216–222.

Jung, S., Jones, T.D., Lugo, J.N., Jr., Sheerin, A.H., Miller, J.W., D'Ambrosio, R., Anderson, A.E., and Poolos, N.P. (2007). Progressive dendritic HCN channelopathy during epileptogenesis in the rat pilocarpine model of epilepsy. J. Neurosci. *27*, 13012–13021.

Lee, H.Y., Ge, W.P., Huang, W., He, Y., Wang, G.X., Rowson-Baldwin, A., Smith, S.J., Jan, Y.N., and Jan, L.Y. (2011). Bidirectional regulation of dendritic voltage-gated potassium channels by the fragile X mental retardation protein. Neuron *72*, 630–642.

Magee, J.C. (1998). Dendritic hyperpolarization-activated currents modify the integrative properties of hippocampal CA1 pyramidal neurons. J. Neurosci. *18*, 7613–7624.

Magee, J.C. (1999). Dendritic Ih normalizes temporal summation in hippocampal CA1 neurons. Nat. Neurosci. *2*, 508–514.

Narayanan, R., and Johnston, D. (2007). Long-term potentiation in rat hippocampal neurons is accompanied by spatially widespread changes in intrinsic oscillatory dynamics and excitability. Neuron *56*, 1061–1075.

Otmakhova, N.A., and Lisman, J.E. (2004). Contribution of Ih and GABAB to synaptically induced afterhyperpolarizations in CA1: a brake on the NMDA response. J. Neurophysiol. *92*, 2027–2039.

Pfeiffer, B.E., and Huber, K.M. (2007). Fragile X mental retardation protein induces synapse loss through acute postsynaptic translational regulation. J. Neurosci. *27*, 3120–3130.

Poolos, N.P., Migliore, M., and Johnston, D. (2002). Pharmacological upregulation of h-channels reduces the excitability of pyramidal neuron dendrites. Nat. Neurosci. *5*, 767–774.

Santoro, B., Chen, S., Luthi, A., Pavlidis, P., Shumyatsky, G.P., Tibbs, G.R., and Siegelbaum, S.A. (2000). Molecular and functional heterogeneity of hyperpolarization-activated pacemaker channels in the mouse CNS. J. Neurosci. *20*, 5264–5275.

Santoro, B., Wainger, B.J., and Siegelbaum, S.A. (2004). Regulation of HCN channel surface expression by a novel C-terminal protein-protein interaction. J. Neurosci. *24*, 10750–10762.

Shin, M., and Chetkovich, D.M. (2007). Activity-dependent regulation of h channel distribution in hippocampal CA1 pyramidal neurons. J. Biol. Chem. *282*, 33168–33180.

Shin, M., Brager, D., Jaramillo, T.C., Johnston, D., and Chetkovich, D.M. (2008). Mislocalization of h channel subunits underlies h channelopathy in temporal lobe epilepsy. Neurobiol. Dis. *32*, 26–36.

Silva, A.J., Stevens, C.F., Tonegawa, S., and Wang, Y. (1992). Deficient hippocampal long-term potentiation in alpha-calcium-calmodulin kinase II mutant mice. Science *257*, 201–206.

Tsay, D., Dudman, J.T., and Siegelbaum, S.A. (2007). HCN1 channels constrain synaptically evoked Ca2+ spikes in distal dendrites of CA1 pyramidal neurons. Neuron *56*, 1076–1089.

Turrigiano, G. (2011). Too many cooks? Intrinsic and synaptic homeostatic mechanisms in cortical circuit refinement. Annu. Rev. Neurosci. *34*, 89–103.

Turrigiano, G.G., and Nelson, S.B. (2000). Hebb and homeostasis in neuronal plasticity. Curr. Opin. Neurobiol. *10*, 358–364.

van Welie, I., van Hooft, J.A., and Wadman, W.J. (2004). Homeostatic scaling of neuronal excitability by synaptic modulation of somatic hyperpolarization-activated Ih channels. Proc. Natl. Acad. Sci. USA *101*, 5123–5128.

Zalfa, F., Giorgi, M., Primerano, B., Moro, A., Di Penta, A., Reis, S., Oostra, B., and Bagni, C. (2003). The fragile X syndrome protein FMRP associates with BC1 RNA and regulates the translation of specific mRNAs at synapses. Cell *112*, 317–327.